

# SELF-KNOWLEDGE DISTILLATION BASED SELF-SUPERVISED LEARNING FOR COVID-19 DETECTION FROM CHEST X-RAY IMAGES

Guang Li<sup>†</sup>   Ren Togo<sup>††</sup>   Takahiro Ogawa<sup>†††</sup>   Miki Haseyama<sup>†††</sup>

<sup>†</sup> Graduate School of Information Science and Technology, Hokkaido University, Japan

<sup>††</sup> Education and Research Center for Mathematical and Data Science, Hokkaido University, Japan

<sup>†††</sup> Faculty of Information Science and Technology, Hokkaido University, Japan

E-mail: {guang, togo, ogawa}@lmd.ist.hokudai.ac.jp, miki@ist.hokudai.ac.jp

## ABSTRACT

The global outbreak of the Coronavirus 2019 (COVID-19) has overloaded worldwide healthcare systems. Computer-aided diagnosis for COVID-19 fast detection and patient triage is becoming critical. This paper proposes a novel self-knowledge distillation based self-supervised learning method for COVID-19 detection from chest X-ray images. Our method can use self-knowledge of images based on similarities of their visual features for self-supervised learning. Experimental results show that our method achieved an HM score of 0.988, an AUC of 0.999, and an accuracy of 0.957 on the largest open COVID-19 chest X-ray dataset.

**Index Terms**— COVID-19, chest X-ray images, self-knowledge distillation, self-supervised learning.

## 1. INTRODUCTION

The Coronavirus 2019 (COVID-19) caused by Severe Acute Respiratory Syndrome Coronavirus 2 (SARS-CoV2) has rapidly spread worldwide, which is declared a global pandemic [1]. As of 16 September 2021, there have been 226,236,577 confirmed cases of COVID-19, including 4,654,548 deaths worldwide<sup>1</sup>. In the light of the unprecedented pandemic by COVID-19, public healthcare systems have faced many challenges such as scarce medical resources, which are pushing healthcare providers to face the threat of infection [2]. Considering the ominously contagious nature of COVID-19, the early screening for COVID-19 has become increasingly important to prevent the further spread of the disease and reduce the burden on saturated healthcare providers.

Real-time Reverse Transcription Polymerase Chain Reaction (RT-PCR) is currently considered the gold standard for COVID-19 detection [3]. However, RT-PCR is reported with a high false-negative rate and is time-consuming, depriving health authorities of the opportunity of early isolation [4]. Because radiological findings of pneumonia are commonly presented in COVID-19 patients, radiologic examinations are often used for diagnosing COVID-19 [5]. In particular, chest X-ray has advantages in terms of the low cost, short scan time, and a low dose of radiation compared to Computed Tomography (CT) [6]. Therefore, computer-aided chest radiography diagnosis has a great potential for the fast screening of COVID-19

and analysis of patients' conditions, which may help radiologists under global pandemic [7].

Self-supervised learning has recently attracted widespread attention in machine learning [8]. Unlike supervised learning using manually annotated labels, self-supervised learning benefits from image characteristics (*e.g.*, texture, position, and color) without manually annotated labels [9]. For example, the study [10] plays a jigsaw game on images, and the study [11] predicts the rotation degrees of images. Particularly, self-supervised learning methods based on the Siamese network have been shown to be effective on different medical datasets [12]. These methods define the inputs as two augmented views from one image, then input to the Siamese network and maximize the similarity between the representations of views [13]. Self-supervised learning is considered helpful for medical image processing, and we introduce the self-knowledge distillation for learning better representations of COVID-19 chest X-ray images.

In this paper, we propose a novel self-knowledge distillation based self-supervised learning method for COVID-19 detection from chest X-ray images. Our method can make use of self-knowledge of images based on similarities of their visual features for self-supervised learning. Experimental results show that we can achieve an HM score of 0.988, an AUC of 0.999, and an accuracy of 0.957 on the largest open COVID-19 chest X-ray dataset [14]. Our method may help to prevent the further spread of the COVID-19 and reduce the burden on healthcare providers and radiologists.

Our contributions are summarized as follows.

- We propose a novel self-knowledge distillation based self-supervised learning method for COVID-19 detection from chest X-ray images.
- We realize promising detection results on the largest open COVID-19 chest X-ray dataset.

## 2. SELF-KNOWLEDGE DISTILLATION BASED SELF-SUPERVISED LEARNING

Our method uses triplet networks (a variant of the Siamese network) [15] to learn discriminative representations from chest X-ray images. Figure 1 shows an overview of the proposed method. The proposed method comprises three networks, where the weights of the target network are an exponential moving average (EMA) of the weights of the online network, and the encoders in self-knowledge distillation network (SKD network) and online network share the weights [16]. Our method consists of two modules, a self-supervised learning module and a self-knowledge distillation module. We show the details of the proposed method in the following subsections.

This study was supported in part by AMED Grant Number JP21zf0127004. This study was conducted on the Data Science Computing System of Education and Research Center for Mathematical and Data Science, Hokkaido University.

<sup>1</sup><https://covid19.who.int>

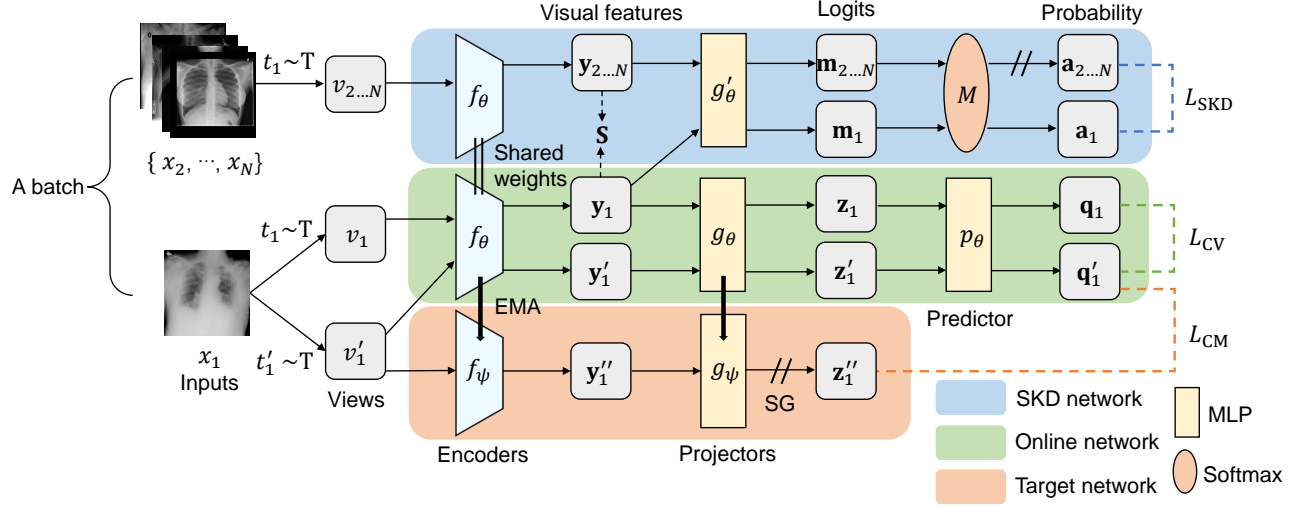


**Fig. 1.** Overview of the proposed method. The weights of the target network ( $\psi$ ) are an exponential moving average (EMA) of the weights of the online network ( $\theta$ ), and the encoders ( $f_\theta$ ) in self-knowledge distillation network (SKD network) and online network share the weights. MLP denotes multilayer perceptron. SG denotes stop-gradient.

## 2.1. Self-Supervised Learning Module

First, we introduce the self-supervised learning module of our method. Given an input chest X-ray image  $x_1$  in a batch of  $N$  images, two transformations  $t_1$  and  $t'_1$  are randomly sampled from the distribution  $T$  to generate two views  $v_1 = t_1(x_1)$  and  $v'_1 = t'_1(x_1)$ . Specifically, these transformations combine standard data augmentation methods such as cropping, resizing, flipping, and Gaussian blur as described in [17]. The view  $v_1$  is processed by the encoder  $f_\theta$  and projector  $g_\theta$  of the online network. Accordingly, the view  $v'_1$  is processed by the encoder  $f_\psi$  and projector  $g_\psi$  of the target network ( $z''_1$  is the final output of  $v'_1$ ). Specifically, we obtain a copy of  $v'_1$  and input it into the online network to calculate the final loss. Furthermore, we use predictor  $p_\theta$  to transform the final outputs of two views as  $\mathbf{q}_1$  and  $\mathbf{q}'_1$  in the online network.

We define the similarity losses between normalized predictions and projections. The cross-view loss  $L_{CV}$  compares the representations of two views from the online network and is defined as follows:

$$L_{CV} = \|\hat{\mathbf{q}}_1 - \hat{\mathbf{q}}'_1\|_2^2 = 2 - 2 \cdot \frac{\langle \mathbf{q}_1, \mathbf{q}'_1 \rangle}{\|\mathbf{q}_1\|_2 \cdot \|\mathbf{q}'_1\|_2}, \quad (1)$$

where  $\hat{\mathbf{q}}_1 = \mathbf{q}_1 / \|\mathbf{q}_1\|_2$  and  $\hat{\mathbf{q}}'_1 = \mathbf{q}'_1 / \|\mathbf{q}'_1\|_2$  denote the normalized predictions of  $v_1$  and  $v'_1$  from the online network, respectively. The cross-model loss  $L_{CM}$  compares the representations of the same view from the online network and the target network and is defined as follows:

$$L_{CM} = \|\hat{\mathbf{q}}'_1 - \hat{\mathbf{z}}''_1\|_2^2 = 2 - 2 \cdot \frac{\langle \mathbf{q}'_1, \mathbf{z}''_1 \rangle}{\|\mathbf{q}'_1\|_2 \cdot \|\mathbf{z}''_1\|_2}, \quad (2)$$

where  $\hat{\mathbf{z}}''_1 = \mathbf{z}''_1 / \|\mathbf{z}''_1\|_2$  denotes the normalized projection of  $v'_1$  from the target network. Note that we only use the predictor in the online network to make the architecture asymmetric, preventing learning from collapsing [18]. We can learn good representations from each chest X-ray image alone with the cross-view loss and the

cross-model loss.

## 2.2. Self-Knowledge Distillation Module

Next, we introduce the self-knowledge distillation module of our method. Self-knowledge distillation can be considered as regularizing the training of a network using soft targets that carry the “dark knowledge” of the same network. Since images with highly similar visual features tend to have similar predicted probabilities, similar images’ knowledge could be ensemble to provide better soft targets for self-knowledge distillation. With the above concept, we can learn better representations from different chest X-ray images based on the similarities of their visual features. As shown in Fig. 1, we first obtain the similarity matrix  $\mathbf{S} \in \mathbb{R}^{N \times N}$  by comparing the encoded visual features  $\{\mathbf{y}_1, \dots, \mathbf{y}_N\}$  in a batch of  $N$  images as follows:

$$\mathbf{S}_{i,j} = (\hat{\mathbf{y}}_i^\top \hat{\mathbf{y}}_j), \quad (3)$$

where  $\hat{\mathbf{y}}_i = \mathbf{y}_i / \|\mathbf{y}_i\|_2$  denotes the normalized representations,  $i, j$  are the indices in the batch, and we discard the diagonal entries with an identity matrix  $\mathbf{I}$  to avoid self-knowledge reinforcement by  $\mathbf{S} = \mathbf{S} \odot (\mathbf{I} - \mathbf{I})$ . Subsequently, we normalize the similarity matrix as follows:

$$\hat{\mathbf{S}}_{i,j} = \frac{\exp(\mathbf{S}_{i,j})}{\sum_{j \neq i} \exp(\mathbf{S}_{i,j})}, \forall i \in \{1, \dots, N\}. \quad (4)$$

The predictive probabilities  $\{\mathbf{a}_1, \dots, \mathbf{a}_N\}$  can be obtained by  $g'_\theta$  and a softmax function  $M$  of the SKD network on the output logits  $\{\mathbf{m}_1, \dots, \mathbf{m}_N\}$  of the SKD network as follows:

$$\mathbf{a}_{(k)} = \frac{\exp(\mathbf{m}_k / \tau)}{\sum_{i=1}^K \exp(\mathbf{m}_i / \tau)}, \quad (5)$$

where  $K$  denotes the dimensions of output logits, and  $\tau$  is a temperature hyperparameter. We denote the predicted probabilities of images within a batch as  $\mathbf{A} = [\mathbf{a}_1, \dots, \mathbf{a}_N]^\top \in \mathbb{R}^{N \times K}$ . To avoid propagating and ensembling noisy predictions too much, we generate the soft targets  $\mathbf{B}$  as a weighted sum of the initial probability

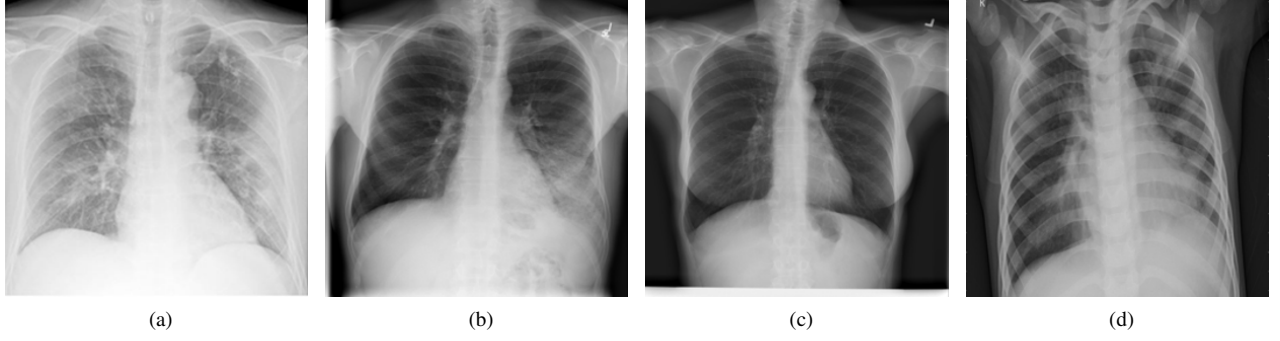


**Fig. 2.** Examples of chest X-ray images: (a) COVID-19, (b) Lung Opacity (c) Normal, and (d) Viral Pneumonia.

matrix  $\mathbf{A}$  and the propagated probability matrix  $\hat{\mathbf{S}}\mathbf{A}$  as follows:

$$\mathbf{B} = \omega \hat{\mathbf{S}}\mathbf{A} + (1 - \omega)\mathbf{A}. \quad (6)$$

And we can propagate multiple times to generate better soft targets  $\mathbf{B}$  for self-knowledge distillation as follows:

$$\begin{aligned} \mathbf{B}_{(t)} &= \omega \hat{\mathbf{S}}\mathbf{B}_{(t-1)} + (1 - \omega)\mathbf{A}, \\ &= (\omega \hat{\mathbf{S}})^t \mathbf{A} + (1 - \omega) \sum_{i=0}^{t-1} (\omega \hat{\mathbf{S}})^i \mathbf{A}, \end{aligned} \quad (7)$$

where  $\omega$  is a weight factor, and  $t$  denotes  $t$ -th propagation and ensembling iteration. When the number of iterations approaches infinite, we have  $\lim_{t \rightarrow \infty} (\omega \hat{\mathbf{S}})^t = 0$  and  $\lim_{t \rightarrow \infty} \sum_{i=0}^{t-1} (\omega \hat{\mathbf{S}})^i = (\mathbf{I} - \omega \hat{\mathbf{S}})^{-1}$ , and hence we can obtain an approximate inference formulation as follows:

$$\mathbf{B} = (1 - \omega)(\mathbf{I} - \omega \hat{\mathbf{S}})^{-1} \mathbf{A}. \quad (8)$$

Finally, we can define the self-knowledge distillation loss  $L_{SKD}$  as follows:

$$L_{SKD} = D_{KL}(\mathbf{B} || \mathbf{A}), \quad (9)$$

where  $D_{KL}$  denotes KL divergence. With the self-knowledge distillation loss, we can learn better representations from different chest X-ray images based on the similarities of their visual features.

### 2.3. Network Optimization

Finally, we show how to optimize the networks of our method. The weights of the online network ( $\theta$ ) are updated by minimizing a total loss  $L$  that combines the similarity losses and self-knowledge distillation loss as follows:

$$L = L_{CV} + L_{CM} + \lambda \cdot \tau^2 \cdot L_{SKD}, \quad (10)$$

$$\theta \leftarrow \text{Opt}(\theta, \nabla_{\theta} L, \alpha), \quad (11)$$

where  $\lambda$  is a balance hyperparameter,  $\text{Opt}$  and  $\alpha$  denote the optimizer and the learning rate, respectively. The weights of the target network ( $\psi$ ) are an exponential moving average of the weights of the online network ( $\theta$ ) and are updated as follows:

$$\psi \leftarrow \sigma \psi + (1 - \sigma) \theta, \quad (12)$$

where  $\sigma$  denotes the degree of moving average, and we update weights after every iteration. The gradient is not back-propagated

**Table 1.** Details of the COVID-19 chest X-ray dataset [14] used in our study.

Class	Total	Training image	Test image
COVID-19	3,616	2,893	723
Lung Opacity	6,012	4,810	1,202
Normal	10,192	8,154	2,038
Viral Pneumonia	1,345	1,076	269

through the soft targets and the target network for stable training [19]. After the self-knowledge distillation based self-supervised learning, the encoder of the online network ( $f_{\theta}$ ) can learn discriminative representations from chest X-ray images and can be used for fine-tuning and COVID-19 detection.

## 3. EXPERIMENTS

### 3.1. Dataset and Settings

The dataset used in our research is the largest open COVID-19 chest X-ray dataset [14]. As shown in Table 1, the dataset has 4 classes (*i.e.*, COVID-19, Lung Opacity, Normal, and Viral Pneumonia) with a total number of 21,165 images. We randomly select 80% chest X-ray images as the training set and the remaining 20% as the test set. Figure 2 shows examples of chest X-ray images. All of these images are grayscale and have a resolution of  $224 \times 224$  pixels. We used sensitivity (Sen), specificity (Spe), their harmonic mean (HM), area under the ROC curve (AUC), and four-class classification accuracy (Acc) as evaluation metrics. For Sen, Spe, HM, and AUC, we took COVID-19 as positive and the others as negative.

We used the ResNet50 [20] network as our encoders  $f_{\theta}$  and  $f_{\psi}$ , whose output feature dimension was 2,048 (the output of the final average pooling layer). The optimizer used in our method was an SGD optimizer, whose learning rate  $\alpha$ , momentum, and weight decay were set to 0.03, 0.9, 0.0004, respectively. The projectors  $g_{\theta}$  and  $g_{\psi}$  and predictor  $p_{\theta}$  are multilayer perceptron (MLP) with the same architecture, comprising a linear layer with an output size of 4,096, a batch normalization layer, a ReLU activation function, and a linear layer with an output size of 256 [18]. We took self-supervised learning on the dataset for 40 epochs and fine-tuning on the dataset for 30 epochs. The batch size was 256, and generated view size was 112. Hyperparameters  $\lambda$ ,  $\tau$ ,  $\omega$ ,  $K$ , and  $\sigma$  were set to 1.0, 4.0, 0.5, 4.0, and 0.996, respectively [18, 21].

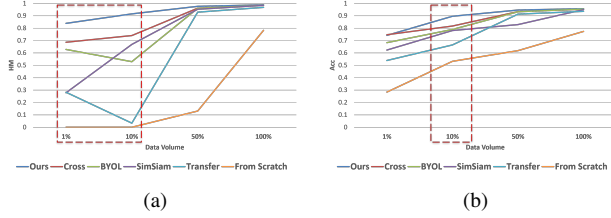
For comparative methods, we used several state-of-the-art self-

**Table 2.** Test results of COVID-19 detection (average of the last 10 fine-tuning epochs).

Method	Sen	Spe	HM	AUC	Acc
Ours	<b>0.980±0.004</b>	<b>0.997±0.001</b>	<b>0.988±0.002</b>	<b>0.999±0.000</b>	<b>0.957±0.001</b>
Cross [22]	0.972±0.003	0.997±0.001	0.985±0.001	0.999±0.000	0.953±0.001
BYOL [18]	0.973±0.004	0.996±0.001	0.985±0.002	0.999±0.000	0.954±0.001
SimSiam [19]	0.974±0.004	0.995±0.001	0.984±0.002	0.998±0.000	0.950±0.001
PIRL-Jigsaw [23]	0.977±0.003	0.997±0.001	0.987±0.001	0.999±0.000	0.951±0.001
PIRL-Rotation [23]	0.973±0.002	0.997±0.001	0.985±0.001	0.999±0.000	0.951±0.001
SimCLR [24]	0.913±0.006	0.994±0.001	0.952±0.003	0.996±0.000	0.936±0.001
Transfer	0.944±0.004	0.994±0.001	0.968±0.002	0.997±0.000	0.936±0.001
From Scratch	0.665±0.013	0.954±0.003	0.783±0.008	0.935±0.001	0.774±0.002

**Table 3.** COVID-19 detection results reported in [14].

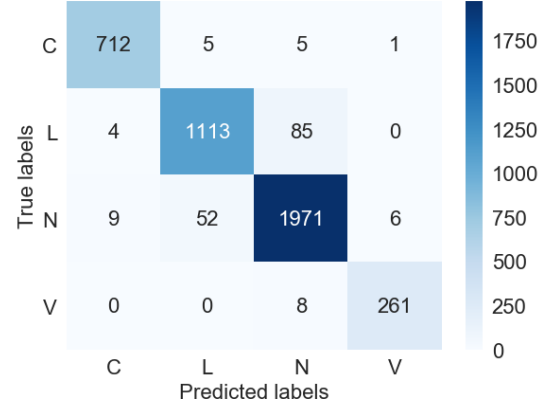
Method	Sen	Spe	HM	Acc
Ours (ResNet50)	<b>0.980</b>	<b>0.997</b>	<b>0.988</b>	<b>0.957</b>
ResNet18	0.934	0.955	0.944	0.934
ResNet50	0.930	0.955	0.942	0.930
ResNet101	0.930	0.951	0.940	0.930
ChexNet	0.932	0.955	0.943	0.932
DenseNet201	0.927	0.954	0.940	0.927
InceptionV3	0.935	0.955	0.945	0.935

**Fig. 3.** Test results of COVID-19 detection in different data volumes: (a) HM and (b) Accuracy.

supervised learning methods such as our self-supervised learning module alone (Cross) [22], BYOL [18], SimSiam [19], PIRL [23], and SimCLR [24]. We also used Transfer learning (using ImageNet [25] pre-trained weights) and training from scratch as baseline methods. To verify the effectiveness of our method with a small amount of data, we randomly selected objects at 1%, 10%, 50%, and 100% of the training set size for the fine-tuning process and COVID-19 detection.

### 3.2. Results and Discussion

Test results of COVID-19 detection are shown in Table 2. We can see that our method outperformed all state-of-the-art self-supervised learning methods. Moreover, the proposed method outperformed the self-supervised learning module alone (Cross), which shows the effectiveness of our self-knowledge distillation module. Table 3 shows COVID-19 detection results reported in [14]. We can see that the proposed method that uses ResNet50 as the backbone drastically outperformed other methods. Figure 3 shows the COVID-19 detection results in different data volumes. From Fig. 3, we can see that our method can significantly improve COVID-19 detection performance in different data volumes compared to other methods, and our method can achieve promising detection performance even us-

**Fig. 4.** Confusion matrix for the best model of our method with an HM score of 0.990, an AUC of 1.000, and an accuracy of 0.959. “C”: COVID-19, “L”: Lung Opacity, “N”: Normal, and “V”: Viral Pneumonia.

ing only 10% data of the training set. Furthermore, Fig. 4 shows the confusion matrix for the best model of our method with an HM score of 0.990, an AUC of 1.000, and an accuracy of 0.959.

Considering the large number of patients who are being screened due to the global pandemic of COVID-19, the use of deep learning for computer-aided diagnosis has strong potential to assist in clinical workflow efficiency and reduce the burden on healthcare providers and radiologists. Our findings show the effectiveness of self-knowledge distillation based self-supervised learning for COVID-19 detection from chest X-ray images. Although the experimental results are promising, the proposed method should be evaluated on other COVID-19 chest X-ray image datasets for any potential bias.

## 4. CONCLUSION

We have proposed a novel self-knowledge distillation based self-supervised learning method for COVID-19 detection from chest X-ray images. Our method can make use of self-knowledge of images based on similarities of their visual features for self-supervised learning. Experimental results show that we realize high detection performance on the largest open COVID-19 chest X-ray dataset. Our method may help to prevent the further spread of the COVID-19 and reduce the burden on healthcare providers and radiologists.

## 5. REFERENCES

- [1] Kristian G Andersen, Andrew Rambaut, W Ian Lipkin, Edward C Holmes, and Robert F Garry, “The proximal origin of sars-cov-2,” *Nature Medicine*, vol. 26, no. 4, pp. 450–452, 2020.
- [2] Qian Liu, Dan Luo, Joan E Haase, Qiaohong Guo, Xiao Qin Wang, Shuo Liu, Lin Xia, Zhongchun Liu, Jiong Yang, and Bing Xiang Yang, “The experiences of health-care providers during the covid-19 crisis in china: a qualitative study,” *The Lancet Global Health*, vol. 8, no. 6, pp. e790–e798, 2020.
- [3] Elisabet Pujadas, Nnaemeka Ibeh, Matthew M Hernandez, Aneta Waluszko, Tatyana Sidorenko, Vanessa Flores, Biana Shiffrin, Numthip Chiu, Alicia Young-Francois, Michael D Nowak, et al., “Comparison of sars-cov-2 detection from nasopharyngeal swab samples by the roche cobas 6800 sars-cov-2 test and a laboratory-developed real-time rt-pcr test,” *Journal of Medical Virology*, vol. 92, no. 9, pp. 1695–1698, 2020.
- [4] Moustapha Dramé, Maturin Tabue Teguo, Emeline Proye, Fanny Hequet, Maxime Hentzien, Lukshe Kanagaratnam, and Lidvine Godaert, “Should rt-pcr be considered a gold standard in the diagnosis of covid-19?,” *Journal of Medical Virology*, 2020.
- [5] Heshui Shi, Xiaoyu Han, Nanchuan Jiang, Yukun Cao, Osamah Alwalid, Jin Gu, Yanqing Fan, and Chuansheng Zheng, “Radiological findings from 81 patients with covid-19 pneumonia in wuhan, china: a descriptive study,” *The Lancet Infectious Diseases*, vol. 20, no. 4, pp. 425–434, 2020.
- [6] Huimin Huang, Ming Cai, Lin, et al., “Graph-based pyramid global context reasoning with a saliency-aware projection for covid-19 lung infections segmentation,” in *Proceedings of the IEEE International Conference on Acoustics, Speech and Signal Processing (ICASSP)*, 2021, pp. 1050–1054.
- [7] Yujin Oh, Sangjoon Park, and Jong Chul Ye, “Deep learning covid-19 features on cxr using limited training data sets,” *IEEE Transactions on Medical Imaging*, vol. 39, no. 8, pp. 2688–2700, 2020.
- [8] Xiao Liu, Fanjin Zhang, Zhenyu Hou, Zhaoyu Wang, Li Mian, Jing Zhang, and Jie Tang, “Self-supervised learning: Generative or contrastive,” *arXiv preprint arXiv:2006.08218*, 2020.
- [9] Longlong Jing and Yingli Tian, “Self-supervised visual feature learning with deep neural networks: A survey,” *IEEE Transactions on Pattern Analysis and Machine Intelligence*, 2020.
- [10] Mehdi Noroozi and Paolo Favaro, “Unsupervised learning of visual representations by solving jigsaw puzzles,” in *Proceedings of the European Conference on Computer Vision (ECCV)*, 2016, pp. 69–84.
- [11] Spyros Gidaris, Praveer Singh, and Nikos Komodakis, “Unsupervised representation learning by predicting image rotations,” in *Proceedings of the International Conference on Learning Representations (ICLR)*, 2018.
- [12] Guang Li, Ren Togo, Takahiro Ogawa, and Miki Haseyama, “Triplet self-supervised learning for gastritis detection with scarce annotations,” in *Proceedings of the IEEE Global Conference on Consumer Electronics (GCCE)*, 2021.
- [13] Guang Li, Ren Togo, Takahiro Ogawa, and Miki Haseyama, “Cross-view self-supervised learning via momentum statistics in batch normalization,” in *Proceedings of the IEEE International Conference on Consumer Electronics – Taiwan (ICCE-TW)*, 2021.
- [14] Tawsifur Rahman, Amith Khandakar, Yazan Qiblawey, Anas Tahir, Serkan Kiranyaz, Saad Bin Abul Kashem, Mohammad Tariqul Islam, Somaya Al Maadeed, Susu M Zughaier, Muhammad Salman Khan, et al., “Exploring the effect of image enhancement techniques on covid-19 detection using chest x-ray images,” *Computers in Biology and Medicine*, vol. 132, pp. 104319, 2021.
- [15] Guang Li, Ren Togo, Takahiro Ogawa, and Miki Haseyama, “Tribyol: Triplet byol for self-supervised representation learning,” in *Proceedings of the IEEE International Conference on Acoustics, Speech and Signal Processing (ICASSP)*, 2022.
- [16] Antti Tarvainen and Harri Valpola, “Mean teachers are better role models: Weight-averaged consistency targets improve semi-supervised deep learning results,” in *Proceedings of the Advances in Neural Information Processing Systems (NeurIPS)*, 2017, pp. 1195–1204.
- [17] Yonglong Tian, Chen Sun, Ben Poole, Dilip Krishnan, Cordelia Schmid, and Phillip Isola, “What makes for good views for contrastive learning,” in *Proceedings of the Advances in Neural Information Processing Systems (NeurIPS)*, 2020, pp. 6827–6839.
- [18] Jean-Bastien Grill, Florian Strub, Florent Altché, Tallec, et al., “Bootstrap your own latent—a new approach to self-supervised learning,” in *Proceedings of the Advances in Neural Information Processing Systems (NeurIPS)*, 2020, pp. 21271–21284.
- [19] Xinlei Chen and Kaiming He, “Exploring simple siamese representation learning,” in *Proceedings of the IEEE Conference on Computer Vision and Pattern Recognition (CVPR)*, 2021, pp. 15750–15758.
- [20] Kaiming He, Xiangyu Zhang, Shaoqing Ren, and Jian Sun, “Deep residual learning for image recognition,” in *Proceedings of the IEEE/CVF Conference on Computer Vision and Pattern Recognition (CVPR)*, 2016, pp. 770–778.
- [21] Yixiao Ge, Ching Lam Choi, Xiao Zhang, Peipei Zhao, Feng Zhu, Rui Zhao, and Hongsheng Li, “Self-distillation with batch knowledge ensembling improves imagenet classification,” *arXiv preprint arXiv:2104.13298*, 2021.
- [22] Guang Li, Ren Togo, Takahiro Ogawa, and Miki Haseyama, “Self-supervised learning for gastritis detection with gastric x-ray images,” *arXiv preprint arXiv:2104.02864*, 2021.
- [23] Ishan Misra and Laurens van der Maaten, “Self-supervised learning of pretext-invariant representations,” in *Proceedings of the IEEE/CVF Conference on Computer Vision and Pattern Recognition (CVPR)*, 2020, pp. 6707–6717.
- [24] Ting Chen, Simon Kornblith, Mohammad Norouzi, and Geoffrey Hinton, “A simple framework for contrastive learning of visual representations,” in *Proceedings of the International Conference on Machine Learning (ICML)*, 2020.
- [25] Jia Deng, Wei Dong, Richard Socher, Li-Jia Li, Kai Li, and Li Fei-Fei, “Imagenet: A large-scale hierarchical image database,” in *Proceedings of the IEEE Conference on Computer Vision and Pattern Recognition (CVPR)*, 2009, pp. 248–255.